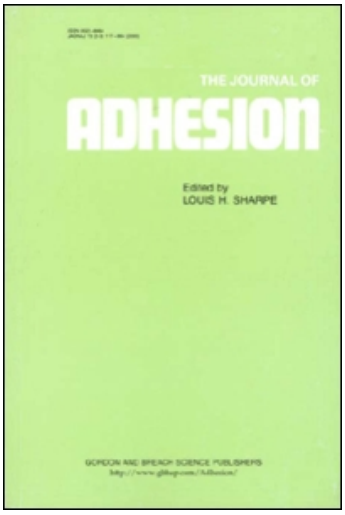

The Journal of Adhesion

Publication details, including instructions for authors and subscription information:
http://www.informaworld.com/smpp/title~content=t713453635

Strain Distributions in Adhesive Wood Joints

A. G. Zink[a]; R. W. Davidson[b]; R. B. Hanna[c]

[a] Department of Wood Science and Forest Products, Virginia Polytechnic Institute and State University, Blacksburg, Virginia, USA [b] Wood Products Engineering, State University of New York, Syracuse, NY, USA [c] Center for Ultrastructure Studies, State University of New York-Environmental Science & Forestry, Syracuse, New York, USA

To cite this Article Zink, A. G. , Davidson, R. W. and Hanna, R. B.(1996) 'Strain Distributions in Adhesive Wood Joints', The Journal of Adhesion, 56: 1, 27 — 43

To link to this Article: DOI: 10.1080/00218469608010497

URL: http://dx.doi.org/10.1080/00218469608010497

J. Adhesion, 1996, Vol. 56, pp. 27–43
Reprints available directly from the publisher
Photocopying permitted by license only

Strain Distributions in Adhesive Wood Joints

A. G. ZINK

Department of Wood Science and Forest Products, Virginia Polytechnic Institute and State University, Blacksburg, Virginia 24061-0323, USA

R. W. DAVIDSON

Wood Products Engineering, State University of New York, Syracuse, NY 13210, USA

R. B. HANNA

Center for Ultrastructure Studies, State University of New York-Environmental Science & Forestry, Syracuse, New York 13210, USA

(Received April 29, 1995; in final form August 12, 1995)

The influence of overlap length on the strain distribution in a double-lap joint was determined using a computer vision, white light speckle technique. The overlap lengths were 12.7 mm (0.5″) and 38.1 mm (1.5″). This range represents a one-tenth scale of overlap lengths in double-lap joints used in adhesive connections in timber trusses. The side members were 50.8 mm (2″) long and the center member was 88.9 mm (3.5″) long. All joint members were 25.4 mm × 25.4 mm (1″ × 1″) in cross section. The joint members were yellow-poplar (*Liriodendron tulipifera*) wood and the adhesive was a resorcinol-formaldehyde.

Even though the connection was loaded in shear, both transverse and shear strains were shown to exist along the gluelines. These strains were significantly intensified at the ends of the overlap. The strain distributions were altered by the degree of overlap and the level of strain concentration was reduced with increased overlap.

The full-field strain distributions as measured with the new computer vision technique revealed progressive failure development, the eventual failure mode and location, and knowledge of the actual distribution of the strains in the entire joint assembly.

KEY WORDS: Adhesive connections; mechanical testing; strain distribution; double lap joint; computer vision white light speckle technique; bond failure analysis; yellow-poplar wood.

INTRODUCTION

All structures, no matter the materials used, consist of an assembly of members fastened together by connections. Adhesive connections play a prominent role in wood construction. They are found in large structural members such as glued-laminated beams, plywood, and wood I-joists. Adhesion as a physical and chemical action is involved in approximately 70% or more of all wood materials in use today and the percentage is expected to be higher in the future.[1] Engineers working on new concepts for more efficient design of structures have found that bonding wood components together rather than nailing, or in addition to nailing, provides increased load-carrying capacity and increased stiffness in the final structure. In wood and wood-based composite structures, the behavior of the connections is influenced by a wide array of variables and is not fully understood.

Wood is the most widely used construction material in the world. In the U.S. alone we consume as much wood by weight as all metals, all plastics, and all Portland cement combined.[2] Over 95% of U.S. homes are built with wood-framed walls and roofs and about 75% with one or more wood-framed floors. The average single family home requires approximately 8,500 square feet (790 square meters) of structural wood-based panels such as plywood and oriented strandboard.[1] Adhesives in wood construction are used for the manufacture of laminated products, as a means of increasing the structural rigidity of sheathing/joist combinations in floors, installing non-structural panel products, end joining dimension lumber, and repair.

For analysis and design of structural adhesive connections, the physical properties of the adhesive and the stress distributions in and around the connection are necessary parameters. With an understanding of the stress distributions, it is possible to take advantage of the increased load-carrying capacity, versatility, and continuum inherent in adhesive connections. Localized stress concentrations that may significantly reduce the strength and overall integrity of the final structure can be minimized if the distribution is known.

Shear tests are one of the most commonly used methods for stress analysis of structural adhesive connections. The samples are simple mechanically and often closely duplicate the geometry and service conditions for many structural applications. Double-lap shear tests are often used because they minimize the loading eccentricities that are encountered when using single-lap joints. Empirical and analytical studies have determined that when a double-lap joint is loaded in tension or compression, the distribution of stress is not uniform along the gluelines.[3-11] Both shear and normal stresses have been shown to exist that are significantly intensified at the ends of the overlaps due to the bending of the side adherends. The highest stresses are shown to develop at either end of the overlap and the ratios of these peak stresses to the average stress are influenced by the thickness of the adherends, the thickness of the adhesive layer, the stiffness of the adhesive as compared with the adherends, the bending of the adherends, and the overlap length. Of the many factors that influence the stress concentrations at the ends of the overlapped regions, the length of the overlapped region has been found to be highly influential.[3-5,10,12-14]

There are limited experimental data on the influence of overlap length on the distribution of strains in double-lap wood joints and the existing analytical techniques are limited in their application to double-lap wood joints because the assumptions in the models often do not apply to wood members. Due to the widespread use of adhesive connections in structural wood members connected as double-lap joints and a lack of experimental data and applicable analytical studies on the distribution of strain, the objective of this study was to determine the influence of overlap length on the distribution of strain in double-lap wood joints.

BACKGROUND

Experimental Analysis of Stress Distributions in Lap Joints

The first systematic experimental attempts to investigate the stresses in adhesives were made by Mylonas[15] using photoelastic models. Enlarged models of lap joints were

made by sealing a plate of photo-elastically sensitive resin, the "adhesive", between steel plates, the adherends. It follows from the general law of similarity of stress distributions in two-dimensional bodies[16] that the stress concentrations observed on loading this composite are comparable with those in an actual lap joint of the same geometry. The photoelastic analyses revealed that stresses are uniform in the central part of the model adhesive and high near the edges of the steel plates.

The strain distribution in maple glue block shear specimens was examined by Yavorsky and Cunningham[17] using brittle lacquer coatings. The configuration of the strain pattern, and the manner in which it formed during a loading cycle, indicated that high stress concentration exist at the corners of the test specimen and that tensile stresses of varying direction and magnitude act on the plane of the glue joint. The occurrence of strain cracks at very low loads near the corners of the shear block indicated high stresses in these regions. Failure would most probably be initiated in these regions of maximum stress and it is suggested that a stress concentration factor be determined in order to establish the magnitude of stress when failure occurs.

The effect of bending was investigated by McLaren and MacInnes[18] by means of models of joints and moiré fringes. In all cases the fringe pattern had the same general character; the order was a minimum at the center of the joint and increased to a maximum at the corners. The end of the adhesive away from the load was in tension which increased across the end towards the highest value at the end closest to the applied load. The adhesive was shown to have a combination of longitudinal tension and tension or "tearing" stress.

Post *et al.*[19] obtained displacement fields in a thick-adherend lap joint using high-sensitivity moiré. Contour maps of the in-plane displacements parallel and perpendicular to the load were obtained across the adhesive and adherend surfaces. Their results show that the thick-adherend lap joint exhibited nearly constant shear strain in roughtly the entire volume of the adhesive. At the center of the lap joint, displacements and shear strains were nonlinear and time-dependent functions of the average shear stress in the adhesive. Transverse displacements across the adhesive thickness were nonlinear with load and nearly two orders of magnitude smaller than the shear strains.

Stress analysis of bonded nylon-glass fiber composites was conducted by Schroeder[20] using the photoelastic stress analysis technique. She reports that the photoelastic analysis agreed qualitatively with predictions of stress distributions based on linear elastic and linear elastic/perfectly plastic theoretical models. The type of stress pattern that developed was dependent on the amount of fiber stiffening in the adherends. It was also found that the stress concentrations shifted location and sign during the application of load. This is probably due to the change in curvature of the specimen as it deflected with increasing load.

Full-Field Strain Measurement

Full-field strain measurement requires determination of strains on the entire surface of the test specimen. Full-field measurement of the distribution of strain in wood and many composites has traditionally been tedious and difficult due, in part, to equipment limitations. Previously, brittle coatings, photoelasticity, moiré methods, and laser speckle interferometry, among others, have been investigated. Each of these methods

requires surface treatments and/or modifications which change the mechanical properties on a local level or require complex and intensive preparation and equipment. Because of the complexity and expense of these methods, examination of only a few specimens is economically possible.

The digital image correlation technique (DICT) is a full-field method in experimental mechanics that has been developed recently.[21] The method relies on correlation of pairs of digitized, computerized video images of the surface of a test specimen acquired during load application. The image used as the reference image in the pair is usually acquired at zero load, and the second image in the pair is acquired as the load increases. Through pattern recognition techniques that identify measurement point locations on the images of the test specimens before and after deformation using x, y coordinates, it is possible to measure the displacements of the points as a result of the increased load. The displacement of a point is the difference in the location of the measurement point before the load was applied and its location in the subsequent image after the load was applied. As few as two points may be used; however, for full-field measurement, hundreds of points can be used to span the entire test specimen surface.

Normal strain can be calculated from the displacements as measured with the image technique by dividing the change in distance between the points, *i.e.* the displacements, by the original distance between the points. Shear strain can be calculated as the change in angle between four measurement points defining an elementary block as determined from the displacements of the four points. A thorough description of the theory and equipment required for this technique may be found in the *Handbook on Experimental Mechanics*.[21] DICT has been employed to obtain quantities of interest in rigid body mechanics, dynamics, fluid mechanics, biomechanics, fracture mechanics, and micromechanics.[22–27] The technique has been applied to a vast range of loading, environmental and testing conditions and materials. It is non-contacting, fast and economical. Because of its advantages and wide-spread application, the technique is rapidly becoming well-established in experimental mechanics.

Choi *et al.*[28] have applied DICT and video microscopy for the measurement of full-field displacements and strains in wood and paper. When applied to very small specimens of wood, 1 mm × 1 mm × 4 mm (0.0394″ × 0.0394″ × 0.157″), it was shown that the DICT could be a fast, simple, and accurate method. Full-field deformation of wood test specimens using laser speckle interferometry and digital image processing was applied by Agrawal[29] to study the suitability of the system for monitoring the creep response of wood. The applicability to full-size specimens of wood and wood composites has been investigated by Zink *et al.*[30, 31] Comparisons between strain measurements obtained with the image correlation technique on wood and several independent measurement devices such as a Mann comparator,[28] strain gages,[29] and a mechanical transducer[32] indicate excellent agreement.

EXPERIMENTAL STUDY

Specimen Preparation

All joint specimens were cut from a single board of yellow-poplar (*Liriodendron tulipifera*). This wood was chosen because the relative uniformity in anatomical

structure would minimize variability in the results due to material inhomogeneities. The average moisture content of the wood specimens prior to joint assembly was 9% as determined following ASTM Standard D-2016-83 Ovendry Method.[33] The average specific gravity of the wood was 0.35 as determined following ASTM Standard D-2395-83 Volume by Mercury Immersion Method.[34] The surfaces to be glued were knife-planed just prior to joint assembly and the specimens were weight matched. The adhesive was Borden Chemical Cascophen RS-224 with catalyst FM-146. This adhesive is a structural wood adhesive and is a room-temperature setting, liquid, resorcinol-formaldehyde resin.

The joints were assembled as double-lap shear joints to minimize loading eccentricities due to the load and supports being offset and because this configuration represents many structural wood connections.[14, 35-40] The overlap lengths studied were 12.7 mm (0.5") for eight joint assemblies and 38.1 mm (1.5") for another eight joint assemblies. These overlap lengths are approximately one-tenth scale of overlaps in double-lap joints used in timber trusses.[14] Figure 1 is a diagram of the general joint used in this study. A special gluing jig was prepared to minimize shifting of the joints in the pressure clamps and deviation from the desired overlap length. The assembled joints were removed from the pressure clamps after 24 hours and the ends of the adherends were carefully sawn flat and parallel. The joints were then conditioned in a moisture chamber for 6 days to complete the adhesive cure and bring the wood to the expected equilibrium moisture content obtained in the testing lab.

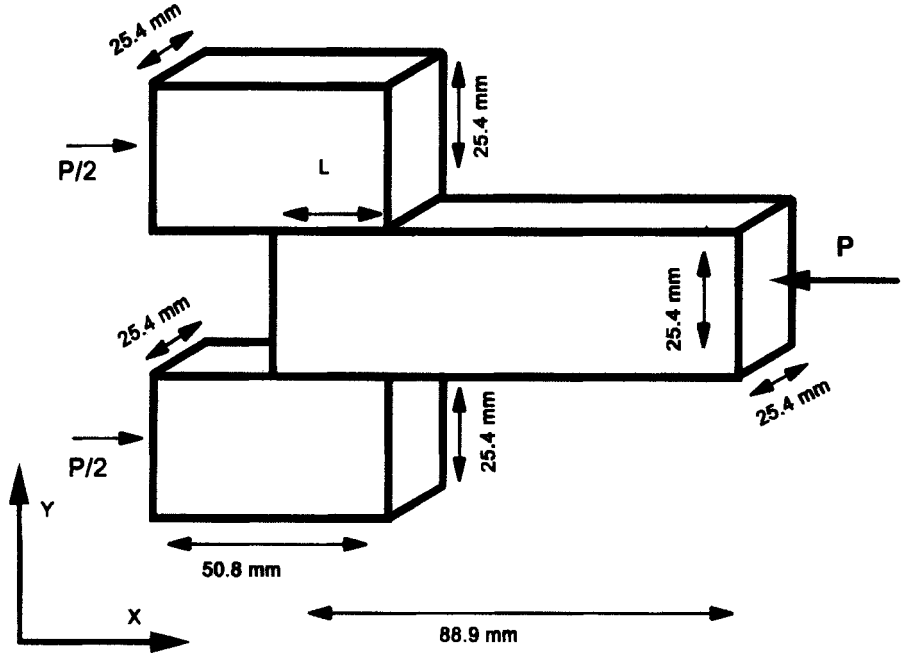

FIGURE 1 Diagram of a typical double lap shear test specimen.

Mechanical Testing

A Baldwin-Emery SR-4 Universal testing machine was used to apply the compression load to the center member of the double lap joints at a cross-head rate of 0.30 mm (0.012″) per minute. The compression load was applied as indicated in Figure 1 parallel to the X-direction. The load data were acquired at a rate of one sample per 0.5 seconds. The full-field displacements were measured with the digital image correlation technique (DICT). The digitizing equipment consisted of a black and white Panasonic WV-CD50 CCD camera and a Coreco Oculus-200 image digitizer board in an IBM PC with a resolution of 480 × 512 pixels. A 55-mm macro lens was used on the video camera for specimen magnification. The white light source was a 22 W circular fluorescent tube suspended and centered around the camera. Variation of the specimen illumination resulting from room and outside light was minimized by extinguishing all room lights and surrounding the testing table and video camera with heavy black cloth and cardboard. Figure 2 is a photograph of a typical testing setup.

The computer vision system was carefully calibrated prior to testing using a linear variable differential transducer and an aluminum compression test block. The accuracy of the system was determined to be ± 0.025% of the full-scale load of 5.08 mm (0.2″) of displacement. System noise was evaluated prior to testing and at random intervals throughout testing to establish baseline noise levels. Distortion from out-of-plane effects were minimized by working with low magnifications (< 3X), a high quality lens

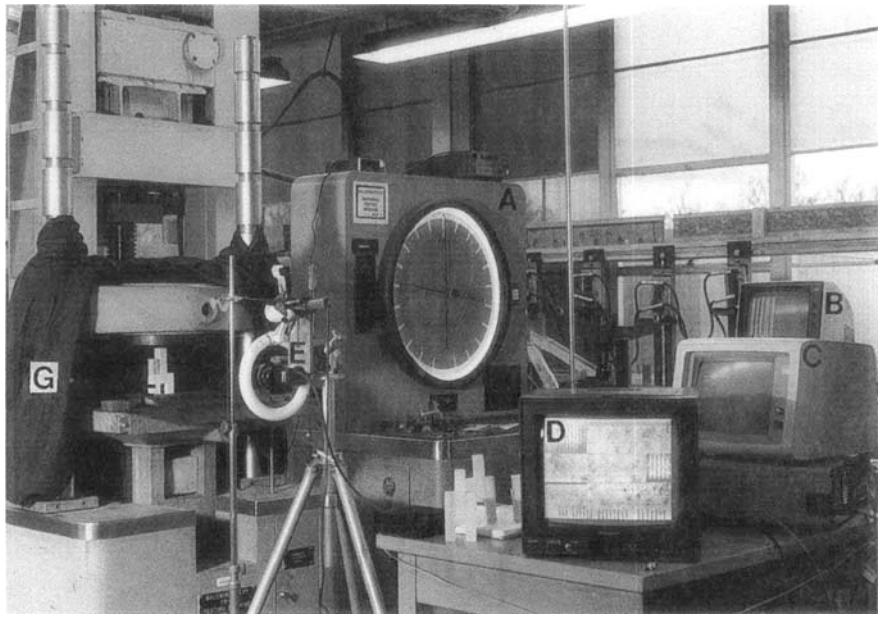

FIGURE 2 Test Set-up for Testing Structural Wood Connections A = Testing Machine, B = Computerized Load Data Acquisition, C = Computer for Image Acquisition, D = Video Display Monitor, E = CCD Video Camera, Lens, and White Light Illumination Source, F = Bonded Wood Double Lap Joint Test Specimen, G = Black Cloth Light Barrier.

with a large depth of field, and specimen-to-lens working distances of > 400 mm. Sutton *et al.*[41] have determined that magnification of $< 5X$ and a distance from the camera lens plane to the object of > 400 mm is sufficient to reduce to an acceptable range any distortion from out-of-plane movement of the specimen. They determined that, at these levels, any noise that appears in the displacement fields is from sources other than out-of-plane effects.

To obtain sub-pixel resolutions, a bilinear interpolation scheme was used to interpolate the gray levels between pixels. The pattern recognition function used for determining the displacements of the selected measurement points was a least squares criterion. In least squares, the sum of the squares of the differences of the light intensity values of sub-regions around the selected measurement points is used to determine the best match to the exact displacements. Convergence optimization was achieved using a quasi-Newton method for successive approximations of the deformation parameters. The normal strain (ε_{yy}) perpendicular to the load between each measurement point was calculated as the change in distance between the points in the y-direction, as measured with the image technique, divided by the original distance between the points ($\Delta L_y/L_y$). The shear strain (ε_{xy}) was calculated as the change in angle between adjacent sides of an elementary block, defined by four points, as this block was distorted under shearing stresses. The change in angle was determined using the displacements of each of the four points of a elementary block as measured with the image technique. The average standard deviation in the strain measurements was $\pm 270\,\mu$ strain. No filtering or noise smoothing of the strain data was employed in this study; however, Sutton *et al.*[42] and Lukasiewicz *et al.*[43] have found that noise can be successfully filtered out of the strain fields using smoothing algorithms.

RESULTS AND DISCUSSION

Strain Distributions- Point-wise Along the Gluelines

A measurement matrix of 9 points parallel to the load and 2 points perpendicular to the load was chosen along the glueline of each specimen. The gauge length between the points parallel to the load was 1.59 mm (0.0625″) for the 12.7 mm (0.5″) overlaps and 4.76 mm (0.187″) for the 38.1 mm (1.5″) overlaps. For the points perpendicular to the load, the gauge length was 0.5 mm (0.02″) for both overlap length specimens. The displacements in the x- and y-direction were measured with the DICT and shear and normal strains calculated from the displacements. The load was applied as a compression load to the center member and parallel to the X-axis as indicated in Figure 1.

Figure 3A is a plot of the shear strain distribution on a point-wise basis along the glueline and Figure 3B is the point-wise normal distribution along the same glueline. The normal strains are strains that occurred in the y-direction and are a result of bending of the side adherends due to non-colinearity of the load and the reactions, and are often called either transverse or tearing strains in the literature. The load at which the data were acquired was 2135 N (480 lbs) for the 12.7 mm (0.5″) overlap specimen and 2264 N (510 lbs) for the 38.1 mm (1.5″) overlap specimen. These loads were chosen because there were well within the elastic range of the load/deflection behavior and to avoid uncertainties due to nonlinear behavior at the onset of failure.

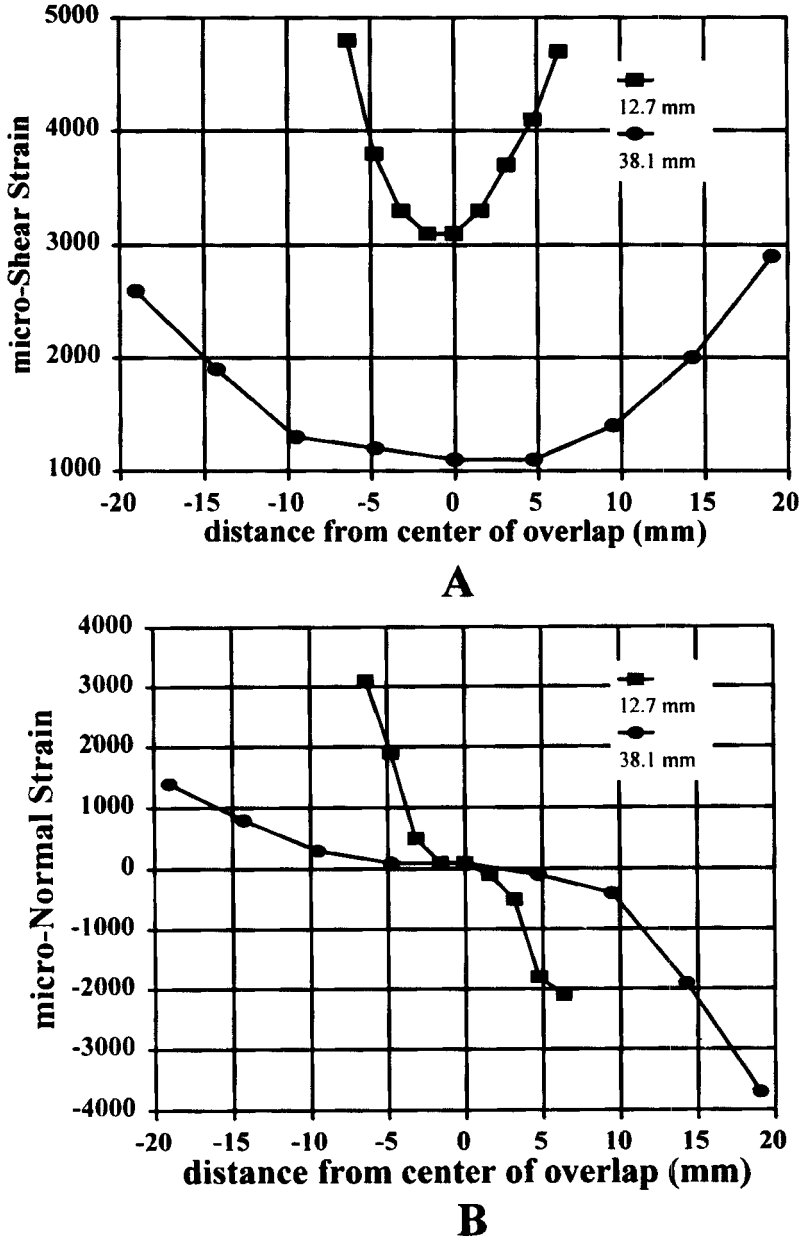

FIGURE 3 μ-Strain Distribution along the gluelines for the 12.7 mm and 38.1 mm overlaps, A = Shear μ-Strain ($\mu\varepsilon_{xy}$) B = Normal μ-Strain ($\mu\varepsilon_{yy}$).

It can be observed from the shear strain distribution in Figure 3A that the distribution along the longer overlap is more uniform than for the shorter overlap. A more uniform distribution of shear strain along the overlap length indicates that the load is more evenly transmitted from the center adherend to the side adherends along

the gluelines. Examination of Figure 3B micro-normal strain indicates that peak tension strain values occur at one end of the glueline and compression strain at the opposite end. The values are nearly zero in the center of both overlap lengths and the compression strains are higher in magnitude than the tension strains due to the differences in wood strength in compression and tension parallel to the grain.

As seen in Figures 3A and B, a very high strain gradient exists at each end of the gluelines in both overlap length specimens. With the shorter length, the shear and normal strains are concentrated in a much shorter span over which to transfer the axial load and a bending moment results from the eccentric loading and glueline rotation. With the longer overlap length, there is a larger region for transfer of load and, as a result, the strains are more evenly distributed along and across the gluelines. These results are in general agreement with those of other studies on the influence of overlap length in composite materials[10, 15, 17-19] and timber trusses.[14]

Shear Strain Concentration Factors

Table I lists a summary of the shear strain concentration factors for total strain from zero load to 2220 N (500 lbs). This load level is still within the elastic range of the load/deflection behavior. The shear strain concentration factor is defined to be the maximum shear strain of the glueline divided by the average glueline shear strain. In this manner, the maximum strain is expressed as a fraction of the average strain. The average concentration factor for the shorter overlap was higher than that for the longer overlap due to the short distance over which the load must be transferred in the shorter overlap length specimens.

In the design of structures, the maximum stress and strain in a particular portion or joint is usually of greater importance than the actual shape of the distribution, since the primary concern is to determine whether the allowable stress will be exceeded under a given loading and not just where this value will be exceeded. For this reason, the concentration factor is an important index of the concentration of stress and strain. Concentration factors have been determined for an array of joint geometries and

TABLE I
Shear Strain Concentration Factors

Overlap Length = 12.7 mm				Overlap Length = 38.2 mm			
Test No.	μShear Max	Strain Ave	Conc Factor	Test No.	μShear Max	Strain Ave	Conc Factor
1	7300	6200	1.18	1	6400	5900	1.08
2	6100	4800	1.27	2	9100	8700	1.05
3	9200	8900	1.03	3	5200	4700	1.11
4	6500	5600	1.16	4	7300	7000	1.04
5	3100	2500	1.24	5	6600	5200	1.27
6	8400	7300	1.15	6	7500	7000	1.07
7	5200	4800	1.08	7	8200	6700	1.22
8	6200	5400	1.15	8	4200	3800	1.11
$\bar{x}$	6500	5688	1.16	$\bar{x}$	6871	6157	1.12
s	1769	1768	0.07	s	1573	1548	0.08

materials; however, to date, only a few concentration factors are available for wood and adhesive joints.

Because only yellow-poplar was used in this study and wood is a naturally variable material, the concentration factors determined in this study are appropriate for yellow-poplar only. While the trend and order of magnitude would be qualitatively applicable to other species and joints, the material and environmental characteristics will have an influence on the actual values and deviations should be expected.

Full-Field Strain Plots

Full-field strain distributions were obtained to monitor the development of failure in the lap joints. Images were recorded at several stages of loading from onset until failure of the joint assembly. The load was applied parallel to the X-axis of the adherends as seen in Figure 1 at a rate of 0.30 mm per minute (0.012″/min). Full-field strain distributions were obtained using a matrix of 16 measurement points along the axis of the adherend (Fig. 1, X-direction) and 19 measurement points perpendicular to the axis (Fig. 1, Y-direction) for a total measurement matrix of 304 points per specimen. The measurement matrix of 304 points was located on the central portion of the test specimen, away from the edges of the test specimen. The gauge lengths for the 12.7 mm (0.5″) overlaps were 4.12 mm (0.162″) in the x-direction and 2.286 mm (0.090″) in the y-direction and, for the 38.1 mm (1.5″) overlaps, they were 5.08 mm (0.200″) in the x-direction and 4.13 mm (0.163″) in the y-direction. The micro normal ($\mu\varepsilon_{yy}$) and micro shear strains ($\mu\varepsilon_{xy}$) were calculated for each measurement point and full-field strain distributions constructed using iso-strain contour lines.

12.7 mm (0.5″) Overlap Specimens

Figures 4-A, B and C are iso-strain contour plots of the micro-normal strains ($\mu\varepsilon_{yy}$) perpendicular to the load (transverse or tearing strains) and micro-shear strains ($\mu\varepsilon_{xy}$) in the 12.7 mm (0.5″) overlap specimens for the central portion of the test specimen, away from the test specimen edges. The load for Figure 4A was 2250 N (510 lbs), for 4B was 4470 N (1004 lbs), and for 4C was 9350 N (2100 lbs). Examination of the shear strain distributions for the 12.7 mm (0.5″) overlap as shown in Figure 4A indicates that, even at a relatively low load level, zones of shear concentration are forming at the corners of the joints even though at this load level the wood components in the joint are still within the elastic range of the mechanical behavior. As seen in all these Figures of the shear strains, one side member is exhibiting positive shear and the other, negative shear. From the conventional definition of the sign of shear strain, this strain pattern is what would be expected from a compression load applied to the center adherend and resisted by supports at the ends of the side adherends.

The effect of increasing the load by a factor of two on the shear strains is illustrated in Figure 4B. The strains are concentrating at the corners of the joints to an even greater degree. Figure 4C illustrates the effect on the shear strain distribution of increasing the load by another factor of two. This load level was just prior to failure of the joint. Figure 4C displays that the shear strain distribution is approximately equal in magnitude and opposite in sign for the side adherends; however, the shear strain in the embedded end of the center adherend is higher in the portion next to the upper side

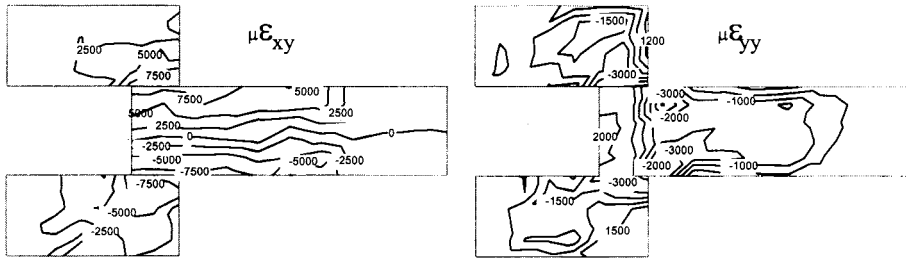

A: Load = 2,250 N

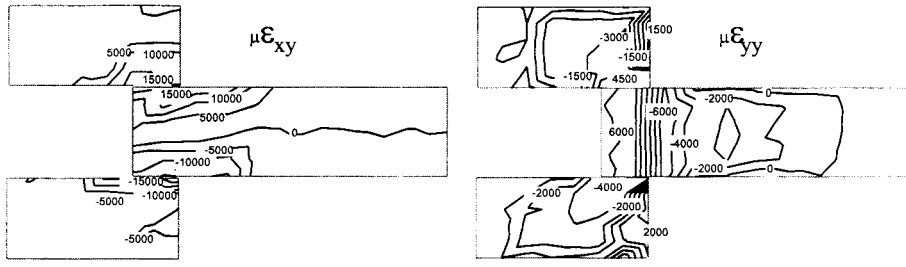

B: Load = 4,470 N

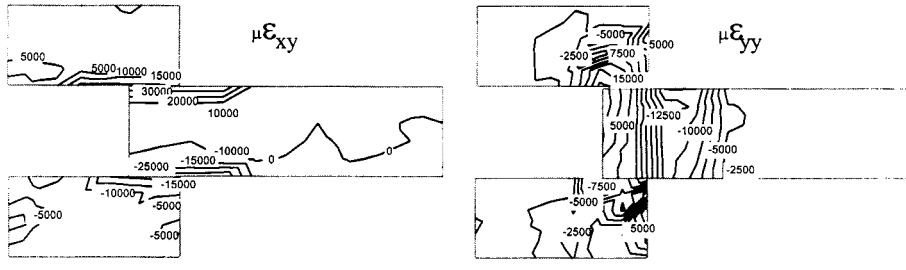

C: Load = 9,350 N

FIGURE 4 Full-field μ-Strain Distributions for the 12.7 mm Overlap Specimen # 13, A: Load = 2250 N, B: Load = 4470 N, C: Load = 9350 N

member than it is in the lower side member. Overall, the highest values of shear strain are located along, or in the vicinity of, the gluelines.

The normal or transverse strains in the vicinity of the glueline in Figure 4A ($\mu\varepsilon_{yy}$) are a result of bending of the side adherends. Because the applied load and the reactions at the supports are not colinear, a bending moment is created that tends to bend the side members concave inward on the center member. As the load level is increased, the transverse strains illustrated in Figure 4B are increasing in value along the glueline and

a region of tension strain is forming at the embedded end of the center adherend. Figure 4C illustrates the effect on the normal strains of increasing the load by another factor of two. This plot indicates an area of very large and highly localized tension strain along the upper glueline in the vicinity of the sharp corner.

Figure 5 is a photograph of the failure specimen used in Figures 4A–C. The failure mode for this specimen was wood cohesive failure due to splitting of the side adherend away from the center adherend. As Figures 4A–C indicated, as the load on the specimen was increased, the adherends began to yield and areas of localized high

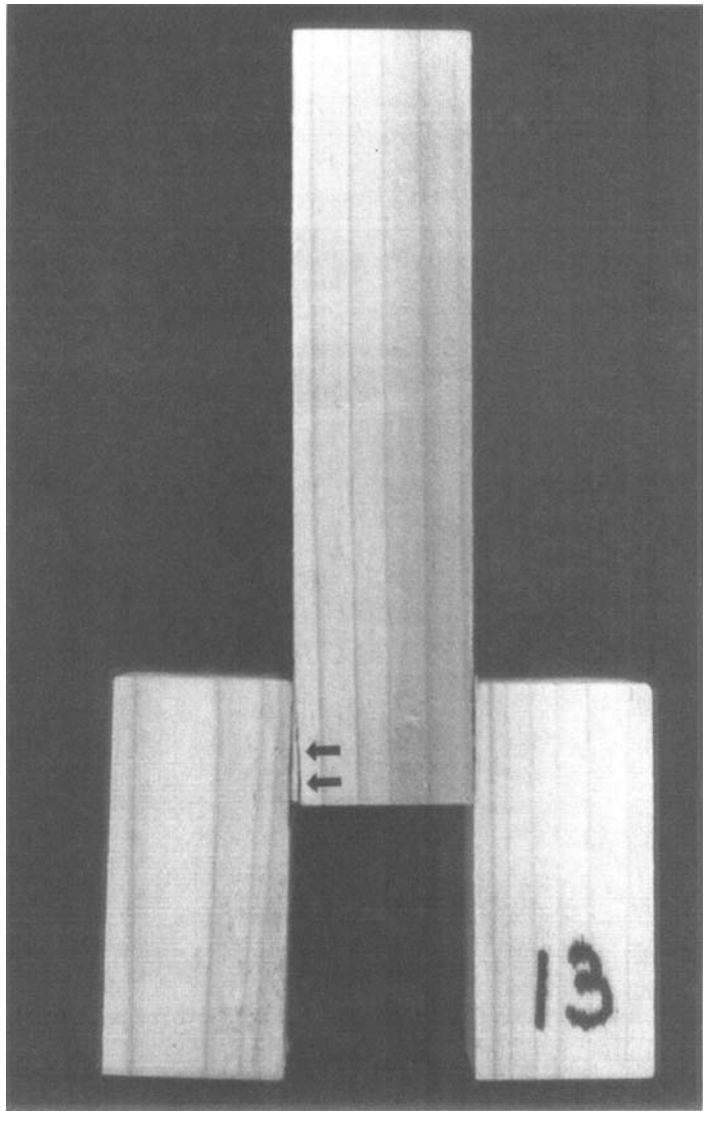

FIGURE 5 Photograph of the Failed 12.7 mm Overlap Specimen #13.

strains developed along the gluelines. The concentration of the adhesive strain at the ends of the gluelines increased due to the yielding in the wood adjacent to the glueline which produced a localized increase in the differential shear effect. Eventually, the local tension perpendicular-to-the-grain strength was exceeded and the center adherend split in the region of the highest strain. Examination of Figure 4C, which was recorded at a load just prior to failure, indicates that the highest strains were in the wood in the vicinity of the gluelines and this is where the joint eventually failed. All specimens tested with an overlap length of 12.7 mm (0.5") failed due to splitting of one or both of the side adherends from the center adherend.

38.1 mm (1.5") Overlap Specimens

Figures 6A, B and C are plots of the shear and normal strains for the 38.1 mm (1.5") overlap length. The load for Figure 6A was 4800 N (1080 lbs), for 6B it was 9180 N (2070 lbs), and for 6C it was 13,360 N (3000 lbs). Examination of the shear strain distribution at the lowest load in Figure 6A indicates that the initial strain state in the double-lap specimen is localized high strains in the regions of the overlaps and the highest values at this load are located in the vicinity of the gluelines. The influence of increasing the load on the shear strain distribution is illustrated in Figure 6B. This plot indicates that the values of shear strain have increased by a factor of two and remain highest in the vicinity of the gluelines. The shear strain distribution is relatively symmetric and opposite in sign for the side members. Increasing the load to 13,360 N (3000 lbs) resulted in accumulation of high shear strain in the regions around the gluelines as seen in Figure 6C. This load was just prior to failure of the joint assembly.

Examination of the normal strains at a load of 4800 N (1080 lbs) as seen in Figure 6A indicates predominantly compression strains at this load; however, an area of high tension strain is forming in the end of the center adherend. These tension strains are a result of the bending of the side adherends due to load eccentricities as described earlier. Figure 6B illustrates the influence of increasing the load to 9180 N (2070 lbs). This plot indicates that the highest tensile strains are accumulating in the bonded end of the center adherend and that the highest compression strains are located at the corners of the joint. The compression in this region is a result of the concave bending of the side adherends. The influence of increasing the load to 13,360 N (3000 lbs) is illustrated in Figure 6C. The iso-strain contour plots of the normal strains as seen in Figures 6A, B and C, show that the highest tension strain is located near the center of the embedded end of the center adherend and localized compression strains are evident at the corners of the joint.

Figure 7 is a photograph of the failed specimen used to create the strain plots shown in Figures 6A–C. The failure mode for the longer overlap specimen was wood cohesive failure due to splitting of the embedded end of the center adherend. Very small regions of compression buckling can be seen at the corners of the joint just beyond the gluelines. Microscopic examination of the failed specimen revealed no visible adhesive cracks or flaws. The absence of flaws and cracks would indicate that the cohesive strength of the adhesive and the adhesive bond had not been exceeded. The failure by splitting of the center adherend is from exceeding the tension perpendicular to the grain strength of the wood.

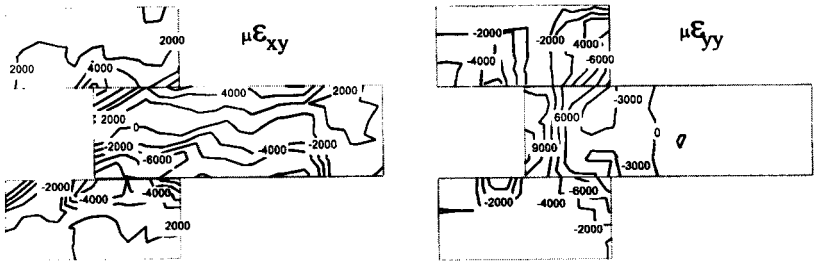

A: Load = 4,790 N

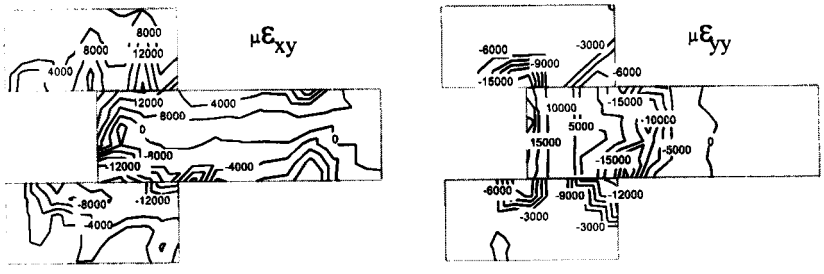

B: Load = 9,180 N

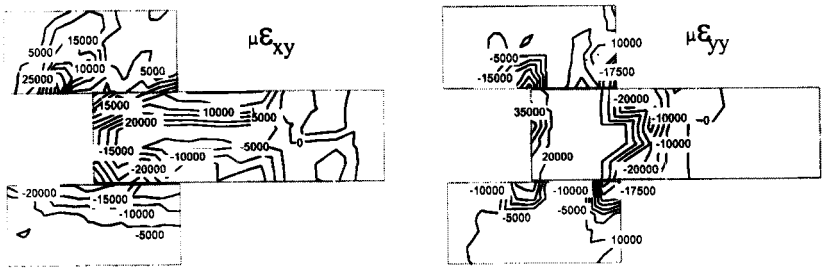

C: Load = 13,400 N

FIGURE 6 Full-field μ-Strain Distributions for the 38.1 mm Overlap Specimen #5, A: Load = 4800 N, B: Load = 9180 N, C: Load = 13, 360 N.

The progressive strain contour plots presented in Figures 6A, B and C indicated that the highest shear strains were near the gluelines and the highest normal strains were at the embedded end of the center adherend. The region of highest normal strain in the longer overlap did not coincide with the location in the shorter overlap length. Because a more uniform transfer of load is expected with the longer overlap length as seen in Figures 3A and B, the load is fully transmitted into the side adherends and the gluelines do not experience shear strain greater than the shear strength of the wood-glue

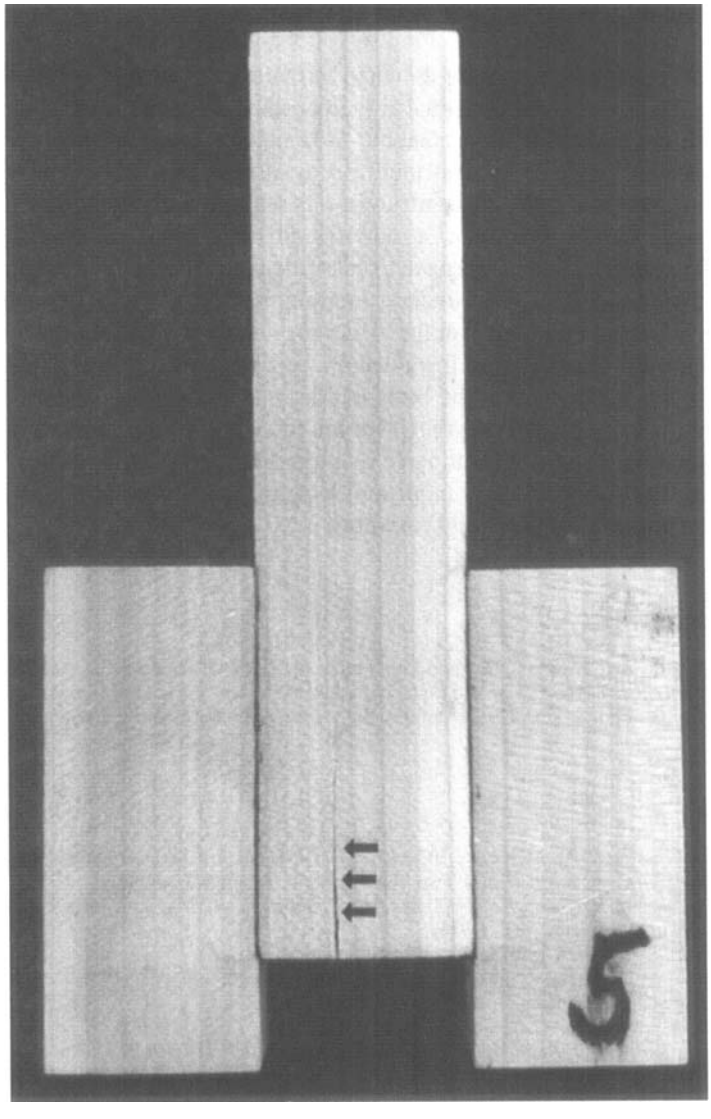

FIGURE 7 Photograph of the Failed 38.1 mm Overlap Specimen #5.

interface or the wood itself. For the wood used in these joints, the tension strength perpendicular to the grain is slightly less than half the shear strength. The combination of bending of the side adherends, the low perpendicular tension strength, and the large tension strains at the end of the center adherend indicates that failure would be expected to occur in this region. Examination of the failed specimen shown in Figure 7 indicates that this is where the specimen eventually failed. All specimens tested with the overlap length of 38.1 mm (1.5″) failed from splitting of the center adherend.

SUMMARY AND CONCLUSIONS

Both normal and shear strains were shown to exist along the gluelines of the double-lap wood joints. These strains were significantly intensified at the ends of the overlaps. The maximum strains at the end of the gluelines were higher than the average strains along the gluelines. The shape of the distribution was altered by a change in the overlap lengths and the level of strain concentration was reduced with an increase in overlap length. Because the distribution of strain was not uniform along the length of the glueline, using the traditional approach to calculate joint strength as the average stress along the gluelines will result in underestimating the actual stress. Disregarding the peak stress values or assuming average values may cause unexpected results.

The sites of peak strains along the gluelines were not the locations of failure of the joints. The failures were within the body of the joint and were due to exceeding the tensile strength perpendicular to the grain for the wood in the joints. The full-field strain measurements using the computer vision technique revealed progressive failure development, the eventual failure mode and location, and knowledge of the distribution of the strains in the entire joint assembly.

Acknowledgements

The authors are grateful to Arnold C. Day and John McKeon, SUNY-CESF, Syracuse, New York, USA, for technical assistance, to Wayne E. Fordyce, Syracuse University, New York, USA, for assistance with the correlation analysis, and to USDA CSRS McIntire-Stennis Program for financial assistance.

References

1. R. G. Anderson and D. B. McKeever, *Wood Used in Residential Construction in the United States*, Market Research Report, American Plywood Association, Tacoma, WA (1991).
2. E. Cliff, *Timber, The Renewable Material, National Commission on Materials Policy*, U.S. Government Printing Office, Washington, D.C. (1973).
3. O. Volkerson, *Luftfahrtforschung* **15,** 41–47 (1938).
4. M. Goland and E. Reissner, *J. Appl. Mech. Trans. ASME* **March,** A17–A27 (1944).
5. W. J. Renton and J. R. Vinson, *J. Adhesion* **7,** 175–193 (1975).
6. F. Delale and F. Erdogan, *J. Appl. Mech. Trans. ASME* **June,** 331–338 (1982).
7. D. Chen and S. Cheng, *J. Appl. Mech. Trans. ASME* **March,** 109–115 (1983).
8. L. J. Hart-Smith, NASA Report CR-112236, Langley Research Center, Hampton, VA (1987).
9. Y. Gilibert, M. L. L. Klein and A. Rigolot, in *Adhesively Bonded Joints: Testing, Analysis, and Design*, **ASTM STP 981,** W. S. Johnson, Ed. (American Society for Testing and Materials, Philadelphia, PA, 1988), pp. 39–53.
10. R. D. Adams, *J. Adhesion* **30,** 219–242 (1989).
11. E. Sancaktar, *J. Adhesion* **34,** 211–220 (1991).
12. N. A. de Bruyne and R. Houwink, *Adhesion and Adhesives* (Elsevier Publishing Company, New York, 1951).
13. R. D. Adams, R. W. Atkins, J. A. Harris and A. J. Kinloch, *J. Adhesion* **20,** 29–53 (1986).
14. P. Glos, D. Henrici and H. Horstmann, *Proceedings of the 1988 International Conference on Timber Engineering*, **September,** Seattle, WA, **1,** 663–672 (1988).
15. C. Mylonas and N. A. de Bruyne, *Adhesion and Adhesives* (Elsevier Publishing Company, New York, 1951), Chap. 4.
16. J. W. Dally and W. F. Riley, *Experimental Stress Analysis*, 3rd Ed. (McGraw-Hill, Inc., New York, 1991), Chap. 12.
17. J. M. Yavorsky and J. H. Cunningham, *Forest Prod. J.* **Feb.,** 80–84 (1955).
18. A. S. McLaren and I. MacInnes, *Brit. J. Appl. Phys.* **9,** 72 (1957).

19. D. Post, R. Czarnek, J. D. Wood and D. Joh, *Adhesively Bonded Joints: Testing, Analysis, and Design*, **ASTM STP 981,** W.S. Johnson, Ed. (American Society for Testing and Materials, Philadelphia, Pennsylvania, 1988), pp. 107–118.
20. J. A. Schroeder, *J. Adhesion* **32,** 89–103 (1990).
21. W. F. Ranson, M. A. Sutton and W. H. Peters, *Handbook on Experimental Mechanics* (Prentice-Hall, Inc., Englewood Cliffs, New Jersey, 1987), Chap. 8.
22. M. A. Sutton, W. J. Wolters, W. H. Peters, W. F. Ranson and S. R. McNeill, *Image and Vision Computing* **1** (No. 3), 133–139 (1983).
23. W. H. Peters and W. F. Ranson, *Optical Engineering* **21,** (No. 3), 427–431 (1982).
24. Z. H. He, M. A. Sutton, W. R. Ranson and W. H. Peters, *Experimental Mechanics* **24,** (No.2), 117–121 (1984).
25. W. F. Ranson, D. M. Walker and J. B. Caulfield " Computer Vision in Engineering Mechanics", A Discussion paper prepared for the NSF Workshop on Solid Mechanics Related to Paper, Blue Mountain Lake, N. Y. (1986).
26. P. F. Luo, Y. J. Chao and M. A. Sutton, *Proceedings 1994 SEM Spring Conference on Experimental Mechanics*, Baltimore, Maryland (1994), pp. 248–253.
27. G. Vendroux, "Scanning Tunneling Microscopy in Micromechanics Investigations", Ph.D. Thesis, California Institute of Technology, Pasadena, CA (1994).
28. D. Choi, J. L. Thorpe and R. B. Hanna, *Wood Sci. & Technol.*, **25,** 251–262 (1991).
29. C. P. Agrawal, "Full-field Deformation Measurement in Wood using Digital Image Processing", M.S. Thesis, Virginia Polytechnic Institute and State University, Blacksburg, Virginia (1989).
30. A. G. Zink, R. B. Hanna and R. W. Davidson, *Wood and Fiber Sci.*, **27,** (No. 4), (1995).
31. A. G. Zink, R. B. Hanna and R. W. Davidson, *Experimental Mechanics* (in review).
32. A. G. Zink "The Influence of Overlap Length on the Stress Distribution and Strength of a Bonded Wood Double Lap Joint", Ph.D. Dissertation, SUNY-CESF, Syracuse, N.Y., (1992).
33. American Society for Testing and Materials, ASTM Standard D2016-83 Method A, Ovendry Method (ASTM, Philadelphia, Pennsylvania, 1986).
34. American Society for Testing and Materials, ASTM Standard D2395-83 Method D, Volume by Mercury Immersion (ASTM, Philadelphia, Pennsylvania, 1986).
35. S. K. Suddarth, Res. Bull. No. 727, Wood Research Lab., Purdue University, Lafayette, IN, (1961).
36. J. R. Goodman, *Wood Sci.* **1** (No. 3), 148–158 (1969).
37. M. L. Selbo, Tech. Bull. No. 1512, USDA Forest Serv., Washington, D.C. (1975).
38. B. H. River and R. H. Gillespie, *Measurement of Shear Modulus and Shear Strength of Adhesives*, FPL Res. Rept., (USDA Forest Serv., Washington, D.C., 1978).
39. G. P. Krueger, *Adhesive Bonding of Wood and Other Structural Materials* (Materials Res. Lab., Pennsylvania State University, University Park, PA, 1981), pp. 321–351.
40. I. C. Bullen, *J. Inst. Wood Sci.* **10,** 220–228 (1986).
41. M. A. Sutton, T. L. Chae, J. L. Turner and H. A. Bruck, **ASTM STP 1094,** MiCon 90 (American Society for Testing and Materials, Philadelphia, Pennsylvania, 1990), pp. 109–132.
42. M. A. Sutton, J. L. Turner, H. A. Bruck and T. A. Chae, *Experimental Mechanics* **31,** (No. 2), 168–177 (1991).
43. S. A. Lukasiewicz, M. Stanuszek and J. A. Czyz, *Experimental Mechanics* **33,** (No. 2), 139–147 (1993).